Supplementary materials

IrCo Nanocactus on Co_xS_y Nanocage as a Highly Efficient and Robust Electrocatalyst for Oxygen Evolution Reaction in Acidic Media

Jun Kim,[ab] Taehyun Kwon,[a] Saerom Yu,[b] So Yeon Chun,[ac] Aram Oh,[d] Jong Min Kim,[b] Hionsuck Baik,[d] Hyung Chul Ham,[be] Jin Young Kim,*[b] Kyungwon Kwak*[ac] and Kwangyeol Lee*[a]

[a]Department of Chemistry and Research Institute for Natural Sciences, Korea University, Seoul 02841, Republic of Korea

[b]Center for Hydrogen & Fuel Cell Research, Korea Institute of Science and Technology (KIST), Seoul 02792, Republic of Korea

[c]Center for Molecular Spectroscopy and Dynamics (CMSD), Institute for Basic Science (IBS), Seoul 02841, Republic of Korea

[d]Korea Basic Science Institute (KBSI), Seoul 02841, Republic of Korea

[e]Department of Chemical Engineering, Inha University, Incheon 22212, Republic of Korea

*Corresponding author: jinykim@kist.re.kr; kkwak@korea.ac.kr; kylee1@korea.ac.kr

Experimental Section

Chemicals and Materials

For the synthesis of materials, cobalt(II) acetate tetrahydrate (ACS reagent, 98%), cobalt(II) nitrate hexahydrate (ACS reagent, ≥98%), hexadecyltrimethylammonium chloride (CTAC, ≥98.0% (NT)), sulfur powder (flakes, 99.5%), iron(III) chloride hexahydrate (ACS reagent, 97%), oleylamine (technical grade, 70%), and 1-octadecene (technical grade, 90%) were purchased from Sigma-Aldrich. Iridium(III) acetylacetonate was purchased from Strem Chemicals. Hydrochloric acid (35%) and acetic acid (Extra pure, 99.5%) was purchased from Daejung Chemicals & Metals. Solvents for washing including toluene, hexane, methanol, ethanol and chloroform were of reagent grade. All chemicals were used as received without further treatment.

Synthesis of CoO@Co_xS_y Core-Shell Octahedral Nanoparticle (COCS NP)

The synthetic procedure for COCS NP is slightly modified from our previous report.[1] In order to synthesize COCS NP, a slurry of cobalt(II) acetate tetrahydrate (0.1992 g) and oleylamine (20.0 mL) was prepared in 250-mL Schlenk tube equipped with a bubbler. The slurry was magnetically stirred at 100 °C for 10 min under O_2 (40%) flow (100 mL/min) to yield transparent violet solution. The violet solution was vigorously stirred and maintained at 290 °C in a hot oil bath for 20 min under O_2 (40%) flow (100 mL/min) to yield CoO octahedral nanoparticles. Then, the reaction tube was cooled down for 10 min under Ar flow (100 mL/min) to remove excess oxygen. For sulfidation, 1.0 M activated elemental sulfur solution (3 mL) was quickly injected into the reaction tube, and the mixture was maintained at 180 °C for 20 min under Ar sealed condition while being vigorously stirred. After the reaction was stopped,

the reaction mixture was cooled down to room temperature and washed with copious amount of toluene and methanol followed by centrifugation at 4000 rpm for 5 min to isolate the final product. The black product was kept under inert condition for later use.

Synthesis of IrCo Nanocactus on Co_xS_y Nanocage (ICS NC)

In order to synthesize ICS NC, a slurry of COCS NP (5 mg), $Ir(acac)_3$ (0.0294 g, 0.06 mmol) and oleylamine (10 mL) was prepared in a 100-mL Schlenk tube with a magnetic stirring. The mixture was placed under sonication for 10 min to yield a homogeneous colloidal suspension, and then evacuated at 100 ^oC for 10 min to remove water and oxygen. After purging the tube with Ar gas, the tube was sealed and placed in a hot oil bath at 250 ^oC for 1 h. Finally, the mixture was cooled down to room temperature and washed with a copious amount of toluene and methanol followed by centrifugation at 4000 rpm for 5 min to isolate the product. The black product was redispersed in hexane/ethanol mixture and 0.1 g of $FeCl_3$ $6H_2O$ was added. The mixture was maintained at 70 ^oC for 1 h while being vigorously stirred to remove any excess Co metal species by redox reaction. Then the mixture was washed several times with a copious amount of ethanol followed by centrifugation at 4000 rpm for 10 min to isolate the product. The final product was dried in a vacuum chamber at room temperature for 12 h.

Synthesis of IrCo Hollow Nanoparticle (IC HNP)

In order to synthesize IC HNP, a slurry of $Co(NO_3)_2$ $6H_2O$ (0.0291 g, 0.1 mmol), $Ir(acac)_3$ (0.0245 g, 0.05 mmol), CTAC (0.0160 g, 0.05 mmol) and oleylamine (10 mL) was prepared in a 100-mL Schlenk tube with a magnetic stirring. The experimental procedure is identical to ICS NC. The initial product is Co@Ir core-shell nanoparticles, and the treatment with $FeCl_3$ solution yield IC HNP.

Material Characterization

Transmission electron microscopy (TEM) images, high-resolution TEM (HRTEM) images, high-angle annular dark-field scanning transmission electron microscopy (HADDF-STEM) images, energy dispersive X-ray spectroscopy (EDS) spectra and elemental mapping images were obtained using Tecnai G2 20 S-Twin microscope operated at 200 kV, Tecnai G2 F30ST microscope operated at 300 kV, and Titan Themis 3 Double Cs & Mono. TEM with Chemi-STEM technology. X-ray diffraction (XRD) patterns were collected with Rigaku Ultima III diffractometer system using graphite-monochromatized Cu-Kα radiation at 40 kV and 30 mA. X-ray photoelectron spectroscopy (XPS) spectra were obtained using PHI 5000 VersaProbe (ULVAC-PHI, Japan) operated at 15 kV and 25 W. The fast Fourier transformation (FFT) patterns were obtained and analyzed from HRTEM images using Gatan Digital Micrograph and TEM Imaging & Analysis software. Raman spectra were obtained using Horiba LabRAM HR Evolution Visible-NIR operated with a 532 nm laser at 3.2 mW focused at 0.41 μm^2 (100x objective), and collection was carried out at an acquisition time of 20 s with 10 times of accumulation. For each sample, the collection was repeated for 3 times at different spots to obtain consistent data.

Electrochemical Characterization

OER activities were measured in N_2-saturated 0.1 M $HClO_4$ using CHI750E (CH Instruments) electrochemical analyzer and rotating disk electrode system (RRDE-3A rotating ring disk electrode apparatus; ALS Co., LTD). For electrochemical characterization, ICS NCs and IC HNPs were mixed with Vulcan XC-72R in chloroform, and the mixtures were put under sonication for 1 h followed by stirring for 2 h. The homogeneous suspension was then treated with acetic acid to remove remaining surfactants on the surface of catalysts. In order to prepare catalyst ink, the catalyst loaded on Vulcan XC-72R was mixed with freshly made D.I. water from Milli-Q Direct 16 Water Purification System, isopropanol and 5 wt% Nafion solution. The volume ratio was 0.7:0.3:0.005. The catalyst ink was placed under sonication for 1 h in a cold water bath to yield a homogeneous ink. Based on ICP-AES analysis, a specific volume for each catalyst ink was dropcasted on a polished glassy carbon disk (5 mm diameter) to load 15 μg cm^{-2} of Ir. A conventional three-electrode system was prepared with the catalyst-loaded 5 mm(ϕ) rotating disk electrode (RDE) as a working electrode, a KCl-saturated silver/silver chloride (Ag/AgCl) electrode as a reference electrode, and a graphite rod as a counter electrode. All the potentials reported in this work were converted to $E_{RHE} = E_{Ag/AgCl} + 0.059*pH + E^o_{Ag/AgCl}$, where $E^o_{Ag/AgCl}$ is equal to 0.197 V at room temperature. The linear sweep voltammetry (LSV) for OER was performed at a scan rate of 5 mV s^{-1} with 95% *iR*-compensation. For chronopotentiometry (CP), catalysts without Vulcan XC-72R were used. To prepare the working electrode for CP, a strip of carbon paper (1 x 8 cm) was coated using two-part epoxy to prevent the carbon paper from soaking, and only the both ends (1 x 1 cm) of the strip were left unprotected for catalyst ink loading and connecting to the electrochemical analyzer. On one end of the epoxy-coated carbon paper strip, a specific volume of each catalyst ink was dropcasted to load 100 μg cm^{-2} of Ir.

Measurement of Electrochemically Active Surface Area (ECSA)

CVs were measured in the potential range of (0.3 ~ 0.5 V vs. RHE) with the scan rates of (10, 20, 40, 80, 120, 160 and 200 mV s^{-1}) and centered currents were used to evaluated as measured charging current (i_c). The ic is equal to the product of multiplication of scan rate (v) and double layer capacitance (C_{dl}), as followed equation (1).

$$i_c = vC_{dl} \quad (1)$$

The ECSA is derived from the equation (2) by dividing the Cdl with specific capacitance (C_s).

$$ECSA = \frac{C_{dl}}{C_s} \quad (2)$$

McCrory *et al*. suggested general specific current density from the previous report.[2] In this work, 0.035 mF cm^{-2} of C_s was used to calculate ECSA.

X-ray absorption spectroscopy

X-ray absorption spectroscopy (XAS) including X-ray absorption near edge structure (XANES) and extended X-ray absorption fine structure (EXAFS) analyses of Ir L_3-edge were conducted by using the beamline 7D of PLS-II, Pohang Accelerator Laboratory (PAL) in Republic of Korea. The monochromatized X-ray from a double crystal monochromator with Si (111) crystals was used for the energy scan. The XAS measurements were performed in fluorescence-transmission geometry, where the spectra were obtained in fluorescence mode, and the spectrum of the reference material placed behind the sample was simultaneously measured in transmission mode at room temperature. The Ir L_3-edge XANES spectra were calibrated to 11215 eV by the reference metallic Ir powders. The white line peak position of XANES spectra were determined by the second derivative of XANES. The XAS raw data were processed using the ATHENA program.

The acquired EXAFS data were processed according to the standard procedures using the ATHENA module implemented in the IFEFFIT software packages. The k^2-weighted EXAFS spectra were obtained by subtracting post-edge background from the overall absorption and then normalizing with respect to the edge-jump step. Subsequently, k^2-weighted $\chi(k)$ data of Ir L_3-edge were Fourier transformed to real (R) space using a Hanning windows (dk = 1.0 $Å^{-1}$) to separate the EXAFS contributions from different coordination shells. To obtain the quantitative structural parameters around central atoms, least squares curve parameter fitting was performed using the ARTEMIS module of IFEFFIT software packages with the *ab initio* code FEFF6.[2,3]

The following equation was used in EXAFS fitting:

$$\chi(k) = \sum_j \frac{N_j S_0^2 F_j(k)}{kR_j^2} \exp\left[-2k^2\sigma_j^2\right] \exp\left[\frac{-2R_j}{\lambda(k)}\right] sin[2kR_j + \phi_j(k)]$$

N_j is the number of neighbors in the j^{th} atomic shell. S_0^2 is the amplitude reduction factor. $F_j(k)$ is the effective curved-wave backscattering amplitude. R_j is the distance between central atom and the atoms in the j^{th} atomic shell (backscatterer). λ is the mean free path in Å. $\phi_j(k)$ is the phase shift. σ_j^2 is the Debye-Waller parameter of the j^{th} atomic shell. For the simulation at the Ir L_3-edge data, the theoretical models used for the EXAFS fitting were generated from the Ir black and IrO_2 structure (Ir-Ir path and Ir-O path).

Computational Methods

The stability and electronic structure of IrO_2 clusters are studied theoretically by using the spin-polarized density functional theory (DFT). All DFT calculations are performed using the Projector Augmented Wave (PAW) method as implemented in the Vienna Ab initio Simulation Package (VASP) and with the Perdew-Burke-Ernzerhof (PBE) functional. The PBE exchange-correlation functional was used with the plane-waves basis set to 400 eV. The Brillouin zone was sampled using a 1 × 1 × 1 Monkhorst–Pack grid for geometry optimization and electronic structure analysis. We prepared a 24-atoms IrO_2 cluster from a 2×2×2 primitive bulk unit cell (a= 4.558 Å / c=3.192 Å, P42/mnm space group) and placed the cluster in the periodic 25 Å × 25 Å × 25 Å cubic box. The model clusters were isolated by at least 7.5 Å from their periodic images in all directions. The size of the 24-atoms IrO_2 cluster was 7.12 Å, 6.71 Å,

and 6.51 Å for x, y, and z direction, respectively. For the sulfur(S)-doped IrO_2 cluster, a S atom was substituted into a lattice oxygen (O) atom. Structural relaxations were performed with the conjugate gradient method until the total energy change between steps and the residual force of each atom become smaller than 10^{-4} eV and 0.02 eV $Å^{-1}$, respectively. The cohesive energy (denoted as E_{coh}) of an Ir atom (which is located at the center position of the octahedral geometry) in the pure IrO_2 and S-doped IrO_2 cases was calculated by the following equation,

$$E_{coh} = E_{iso,\ Ir} + E_{vac,\ Ir} - E_{perfect} \quad (3)$$

where $E_{iso,Ir}$, $E_{vac,Ir}$, $E_{perfect}$ are the total energy of the single isolated Ir atom, the IrO_2 (or S-doped IrO_2) cluster having an Ir vacancy, and the IrO_2 (or S-doped IrO_2) cluster, respectively.

Supplementary Figures

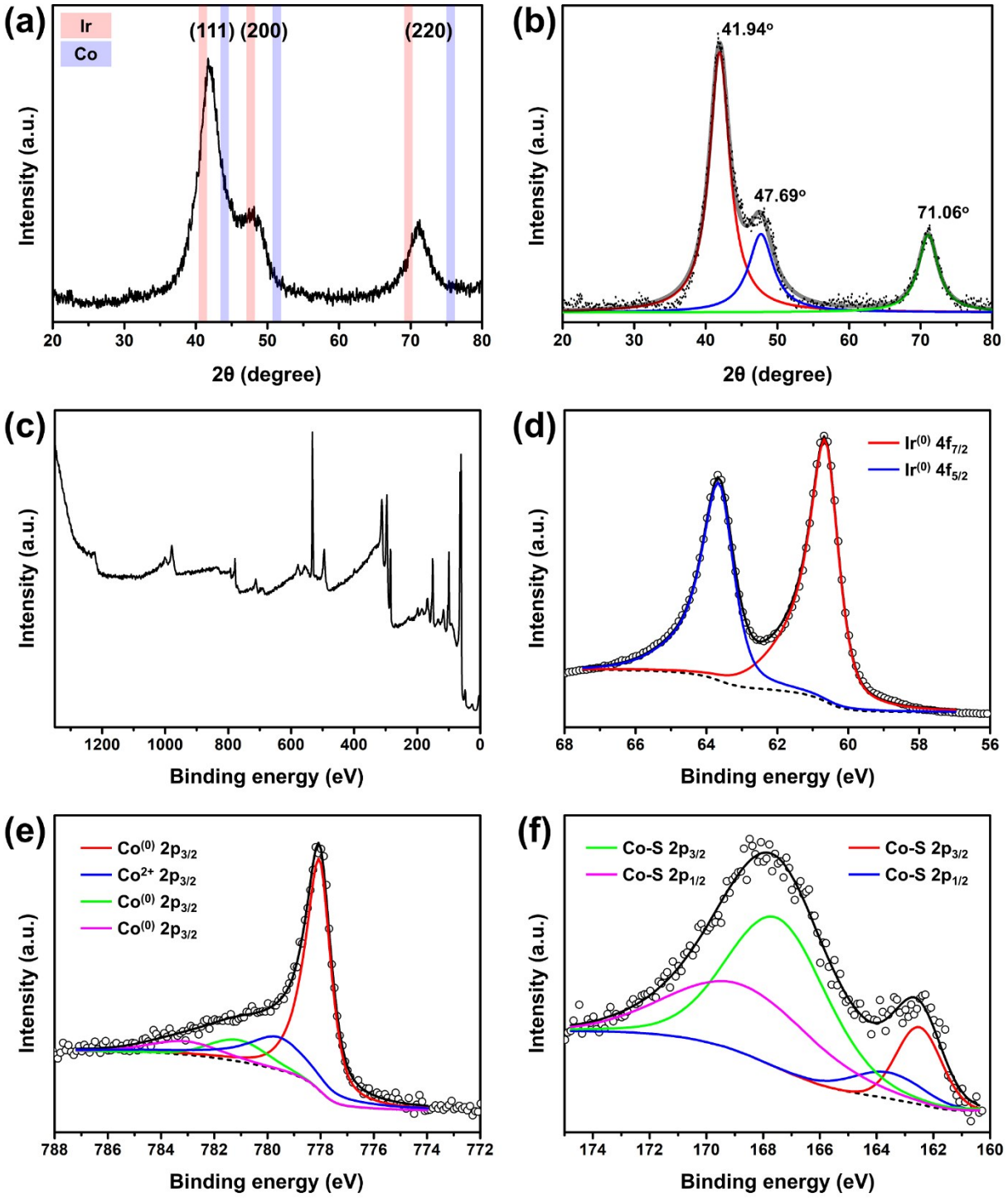

Fig. S1 (a) XRD pattern of **ICS NCs** (Ir: PDF#01-071-4659; Co: PDF#01-071-4651) and (b) the deconvoluted peaks of (a). (c) XPS survey spectrum and XPS analysis of **ICS NCs** for (d) Ir 4f, (e) Co 2p, and (f) S 2p.

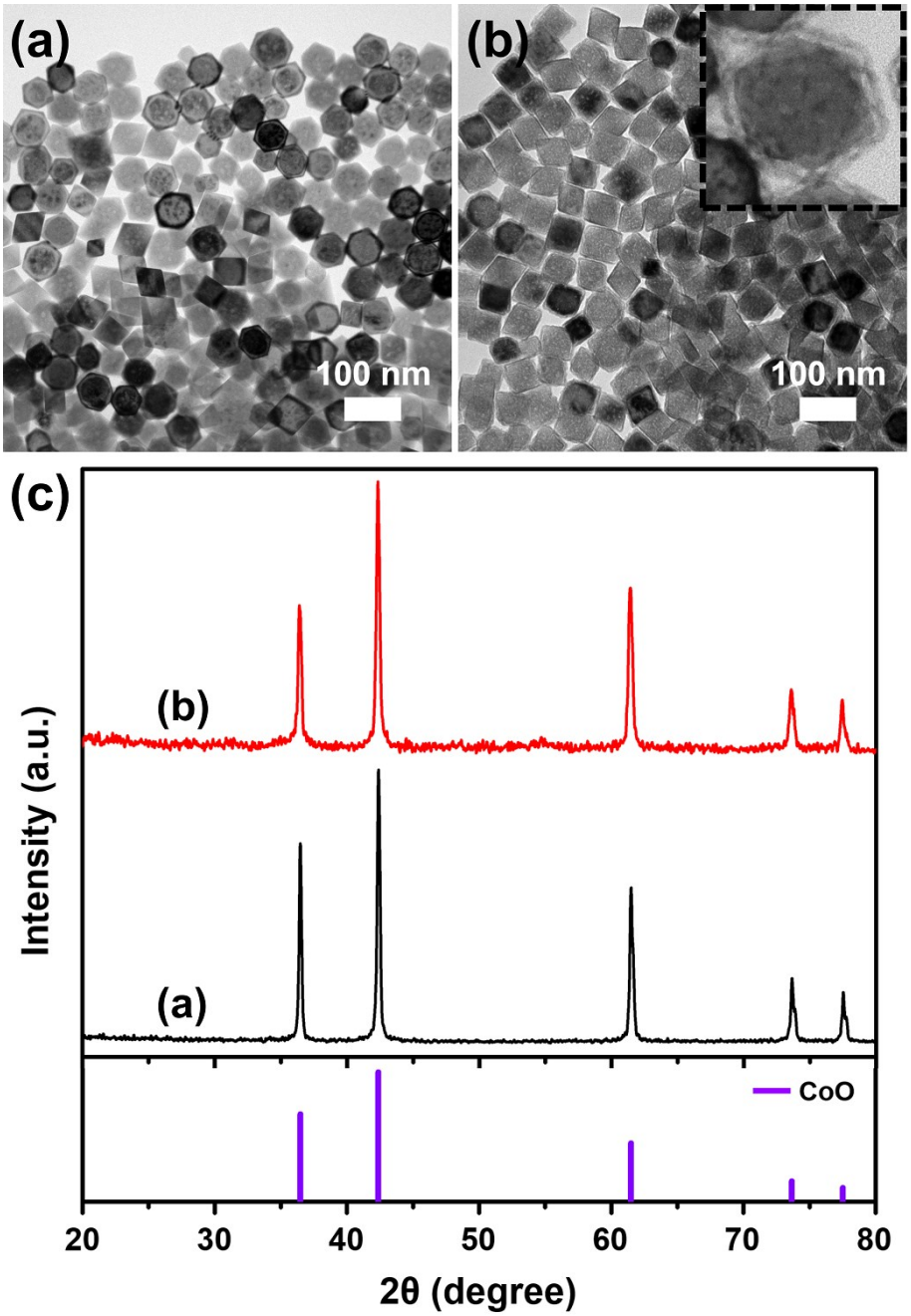

Fig. S2 TEM images of (a) CoO octahedral nanoparticles and (b) **COCS NPs** with an inset showing the magnified image of a **COCS NPs**. (c) XRD patterns of (a) and (b). (CoO: PDF#01-078-0431)

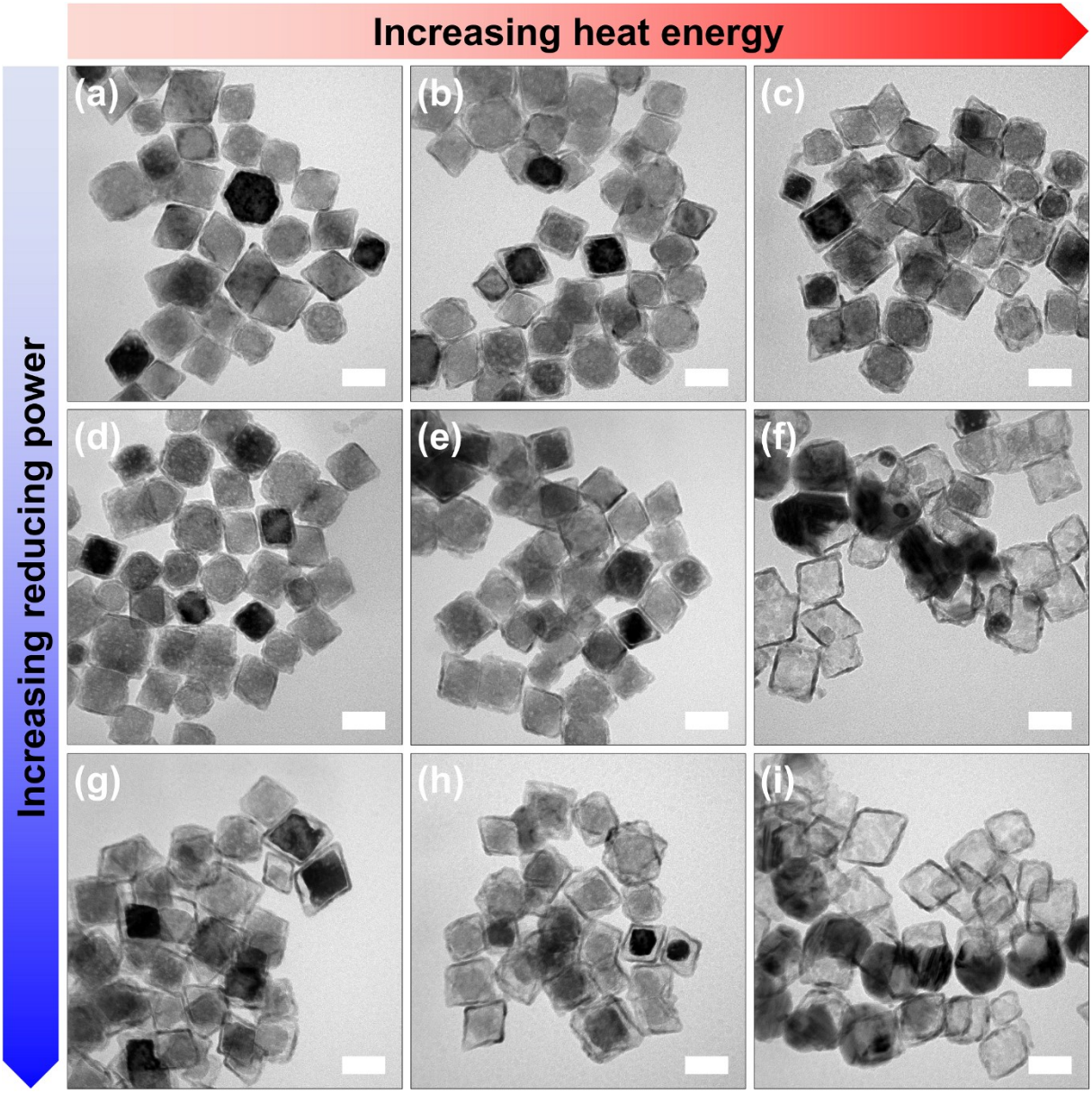

Fig. S3 TEM images showing the metastability of CoO cores in **COCS NPs** depending on the reaction temperature and reducing power of solvent. The experimental procedure is equivalent to that of **ICS NCs** except for the solvent ratio and reaction temperature, and only **COCS NPs** were used as precursors. Fe^{3+} treatment was not performed. The reaction temperatures were (a,d,g) 200 °C, (b,e,h) 220 °C and (c,f,i) 240 °C. The v/v ratios of OAM and ODE were (a,b,c) 1:4, (d,e,f) 2:3, and (g,h,i) 5:0. The scale bars are 50 nm.

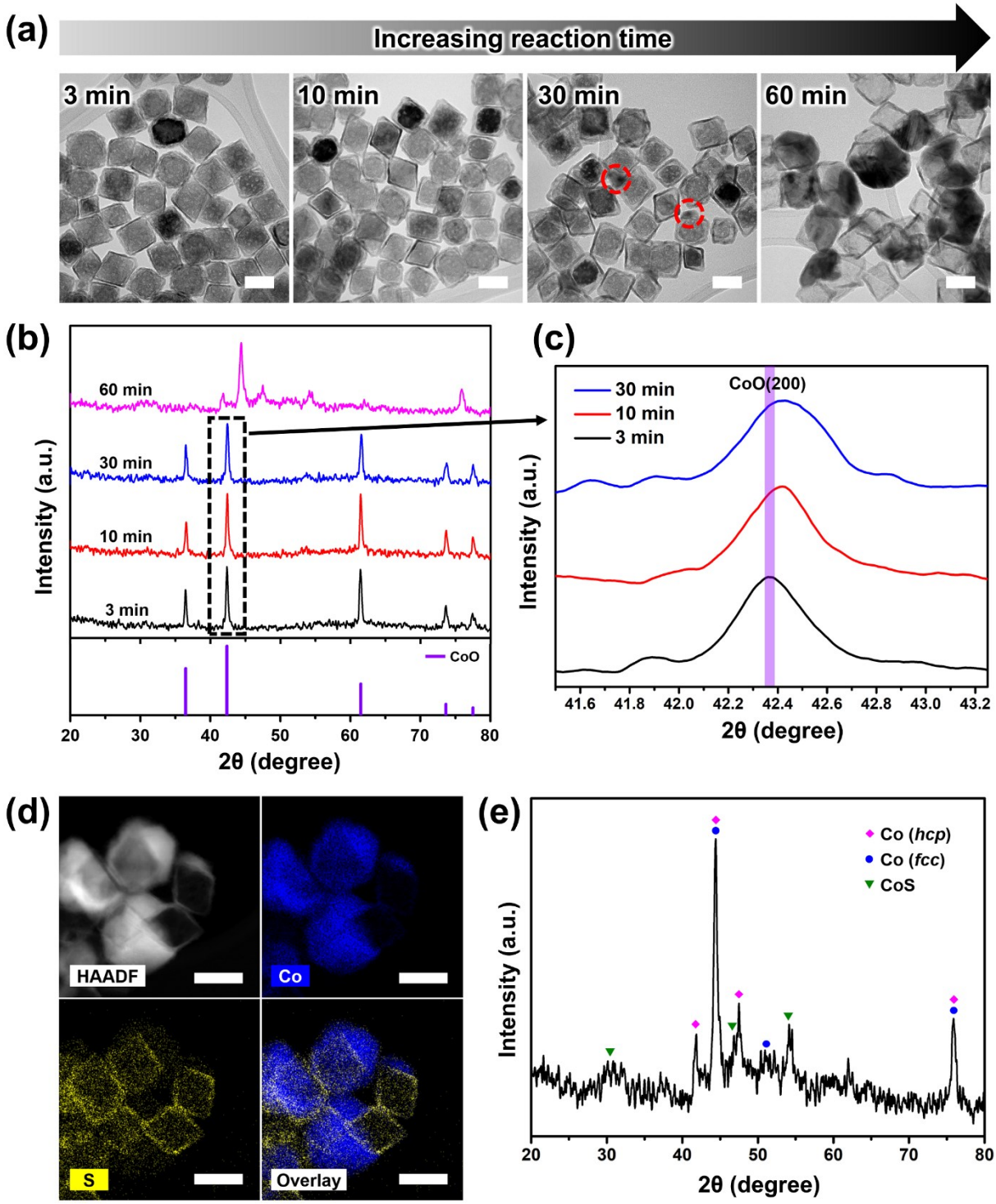

Fig. S4 (a) TEM images showing the decomposition and reduction of CoO cores in **COCS NPs** at intermediate stages and (b) the corresponding XRD patterns for the products shown in (a) (CoO: PDF#01-078-0431). At 30 min, the formation of small Co nanocrystals can be observed in the red circles. (c) The XRD patterns of the selected region (dotted-line box) in (c). (d) HAADF-STEM image, elemental mapping images and (e) XRD pattern of **COCS NPs** after 60 min reaction (Co: PDF#01-071-4651, PDF#01-077-7453; CoS: PDF#01-075-0605). The experimental procedure is equivalent to that of **ICS NCs** except for the reaction time and reaction temperature (240 ^{o}C), and only **COCS NPs** were used as precursors. Fe^{3+} treatment was not performed.

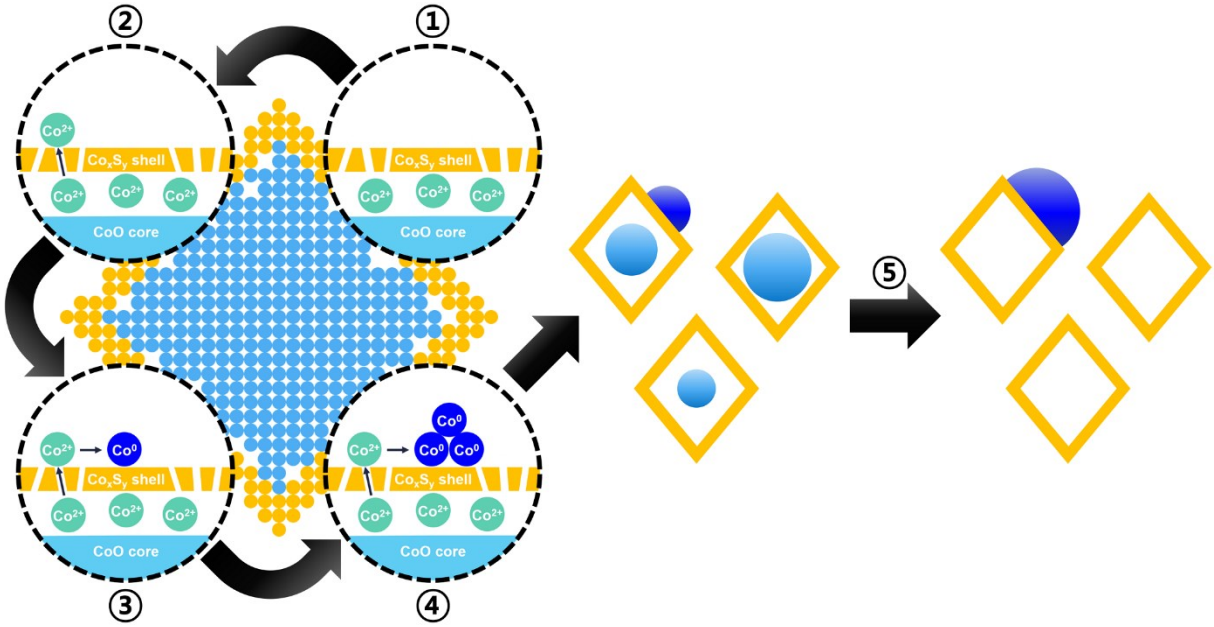

Fig S5 Mechanism of Co nanocrystal formation on the surface of Co_xS_y nanocages from **COCS NPs.** (1) Decomposition of CoO, (2) outward diffusion of Co^{2+} ions through Co_xS_y shell, (3) reduction of Co^{2+} ions to $Co^{(0)}$ atoms, (4) continuous decomposition of CoO and growth of Co nanocrystals, and (5) termination of Co nanocrystal growth.

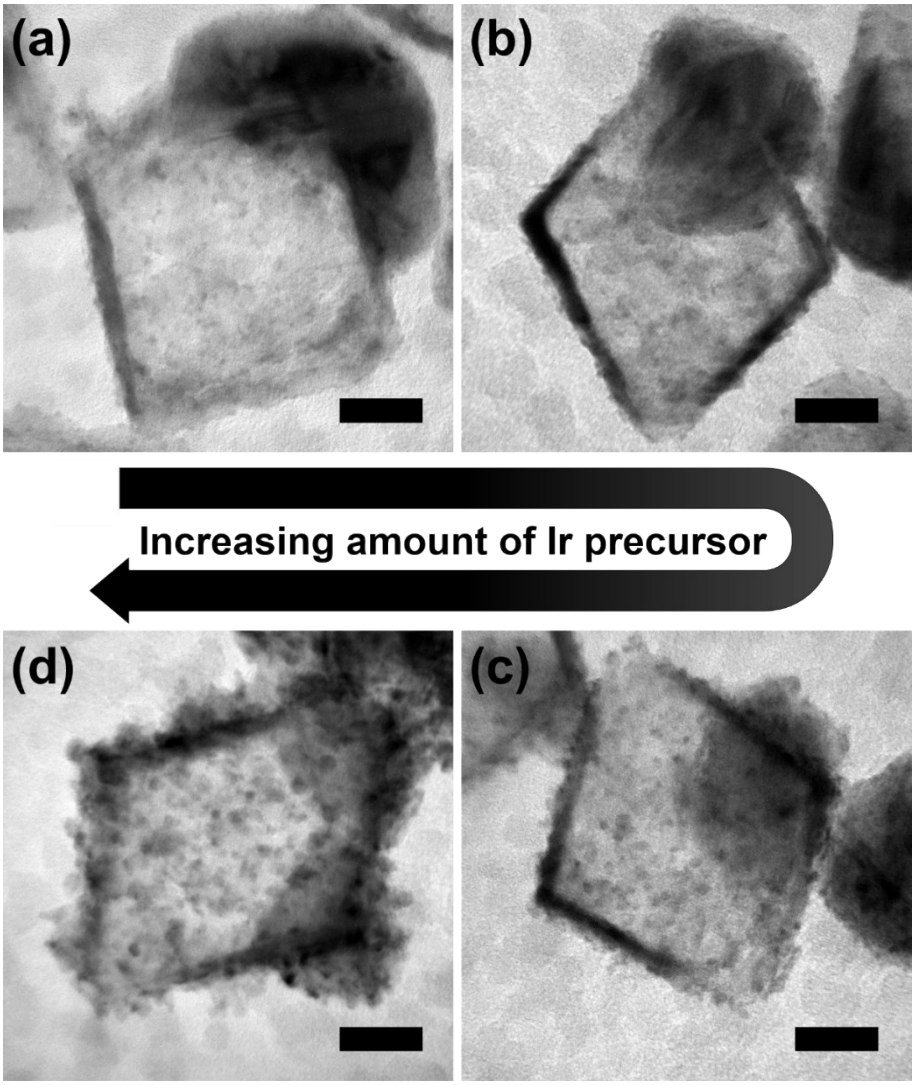

Fig. S6 TEM images of **ICS NCs** synthesized with (a) 0.001 mmol, (b) 0.003 mmol, (c) 0.005 mmol and (d) 0.008 mmol of $Ir(acac)_3$. The large nanocrystal attached on the nanocage is metallic cobalt. Scale bars are 20 nm. The experimental procedure is equivalent to that of **ICS NCs** except for the amount of Ir $(acac)_3$, and Fe^{3+} treatment was not performed.

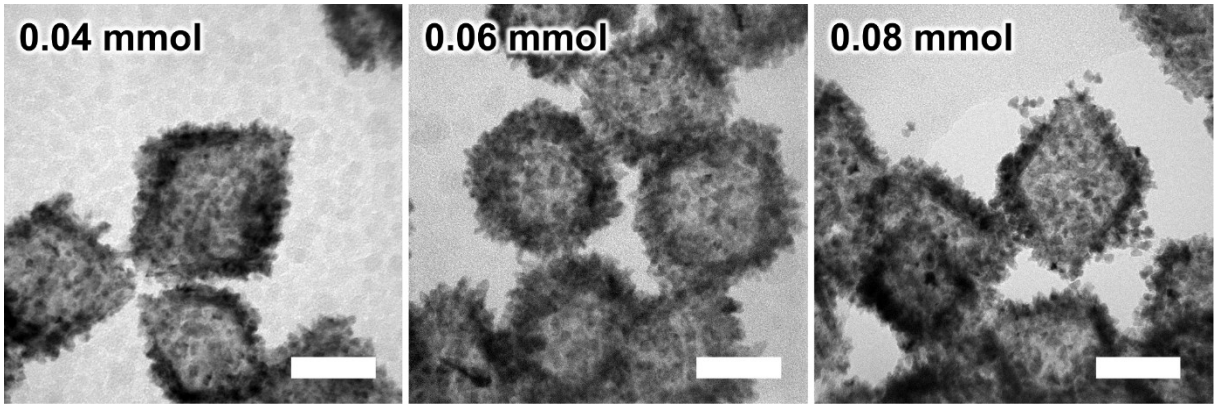

Fig. S7 TEM images of **ICS NCs** synthesized with different amounts of $Ir(acac)_3$ for the optimization of the amount of $Ir(acac)_3$. The experimental procedure is equivalent to that of **ICS NCs** except for the amount of Ir $(acac)_3$, and Fe^{3+} treatment was not performed.

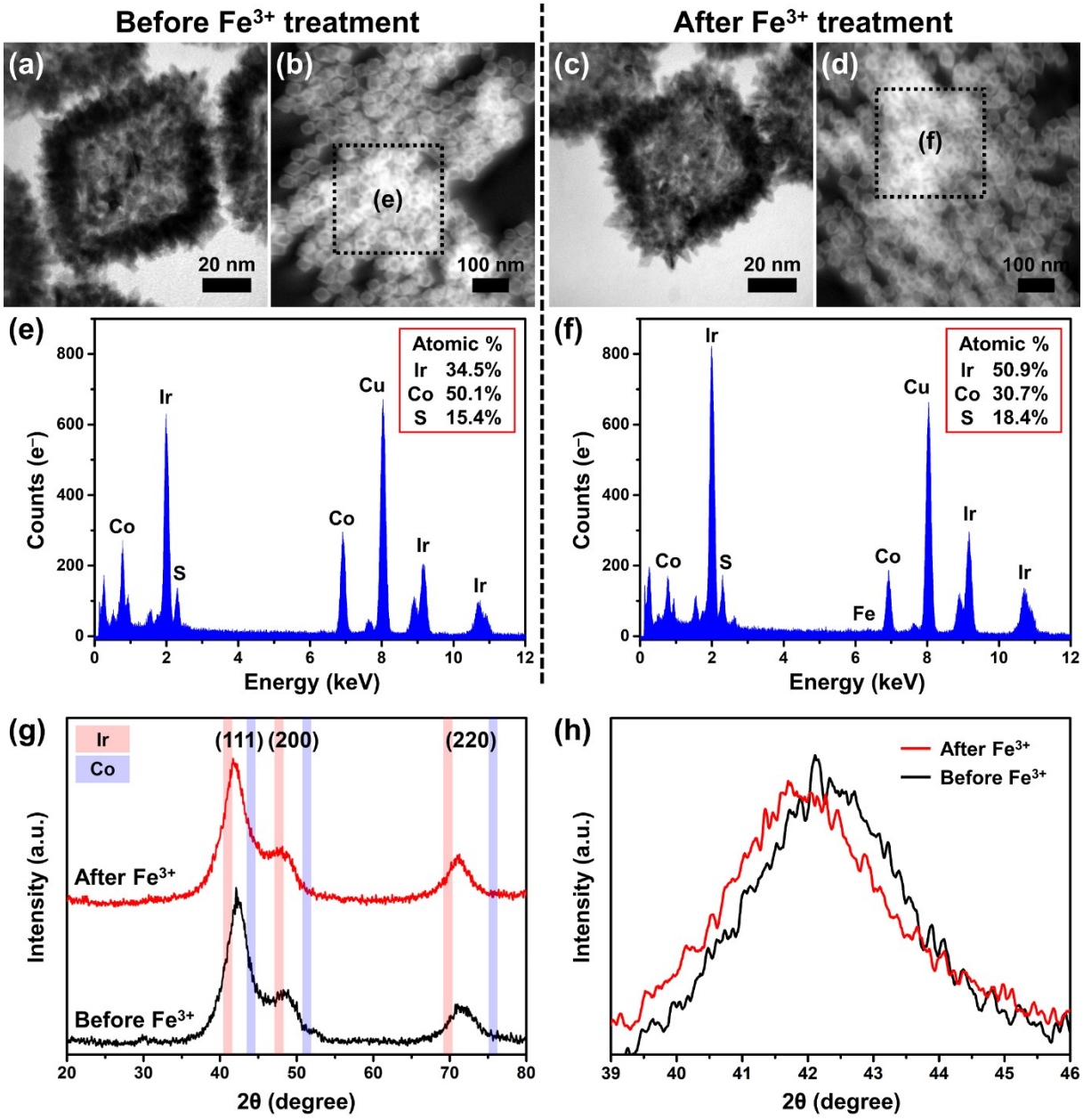

Fig. S8 (a,c) TEM images, (b,d) STEM, and (e,f) EDS analysis of **ICS NCs** before and after Fe^{3+} treatment. Cu detection in EDS due to Cu grid for TEM analysis. (g) XRD patterns of **ICS NCs** before and after Fe^{3+} treatment (Ir: PDF#01-071-4659; Co: PDF#01-071-4651) and (h) showing a narrow range of (g) with overlayed peaks.

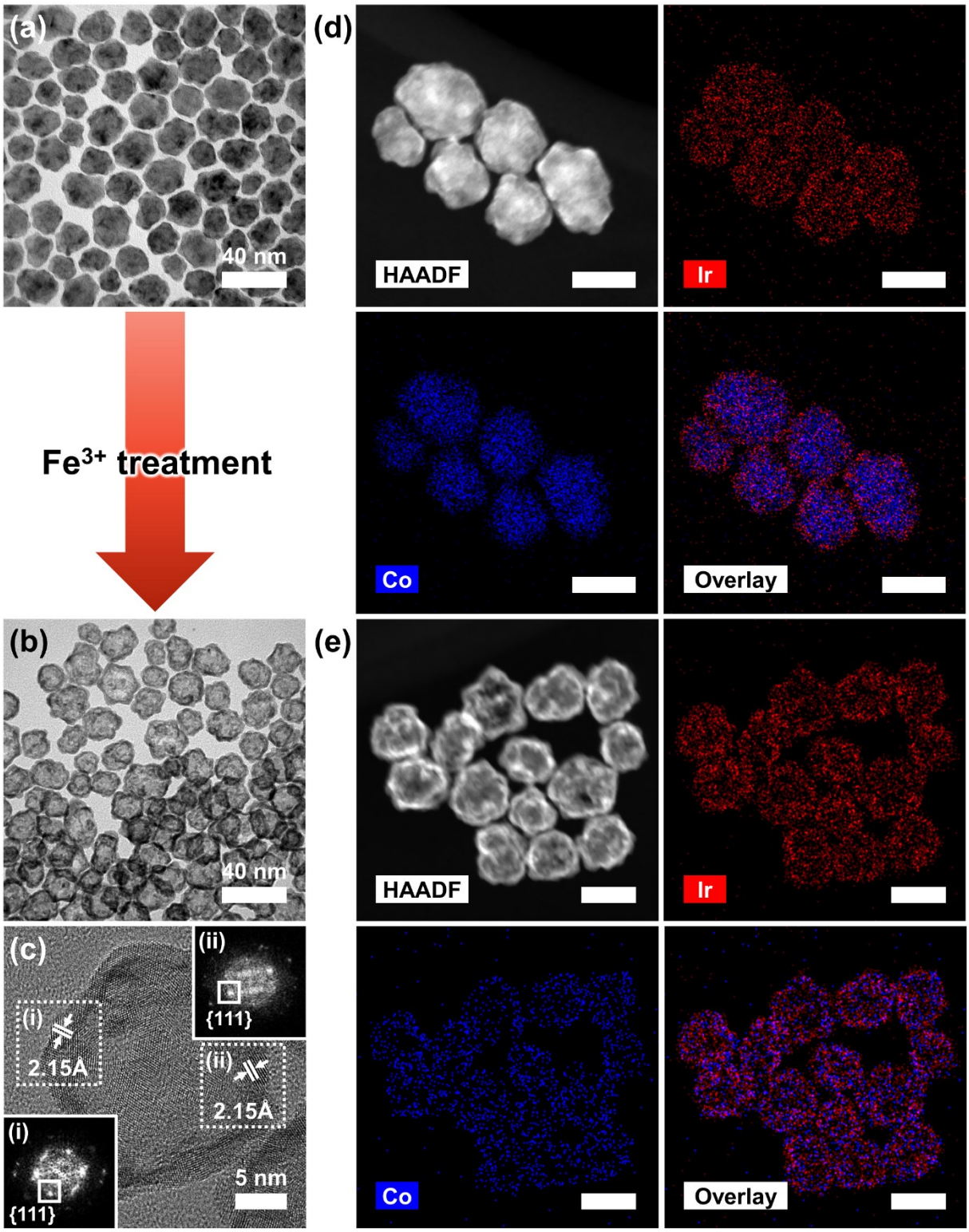

Fig. S9 TEM images of (a) Co@Ir core-shell nanoparticles and (b) IrCo hollow nanoparticles **(IC HNPs).** (c) HRTEM image of an **IC HNP.** Elemental mapping images of (d) Co@Ir core-shell nanoparticles and (e) **IC HNPs.**

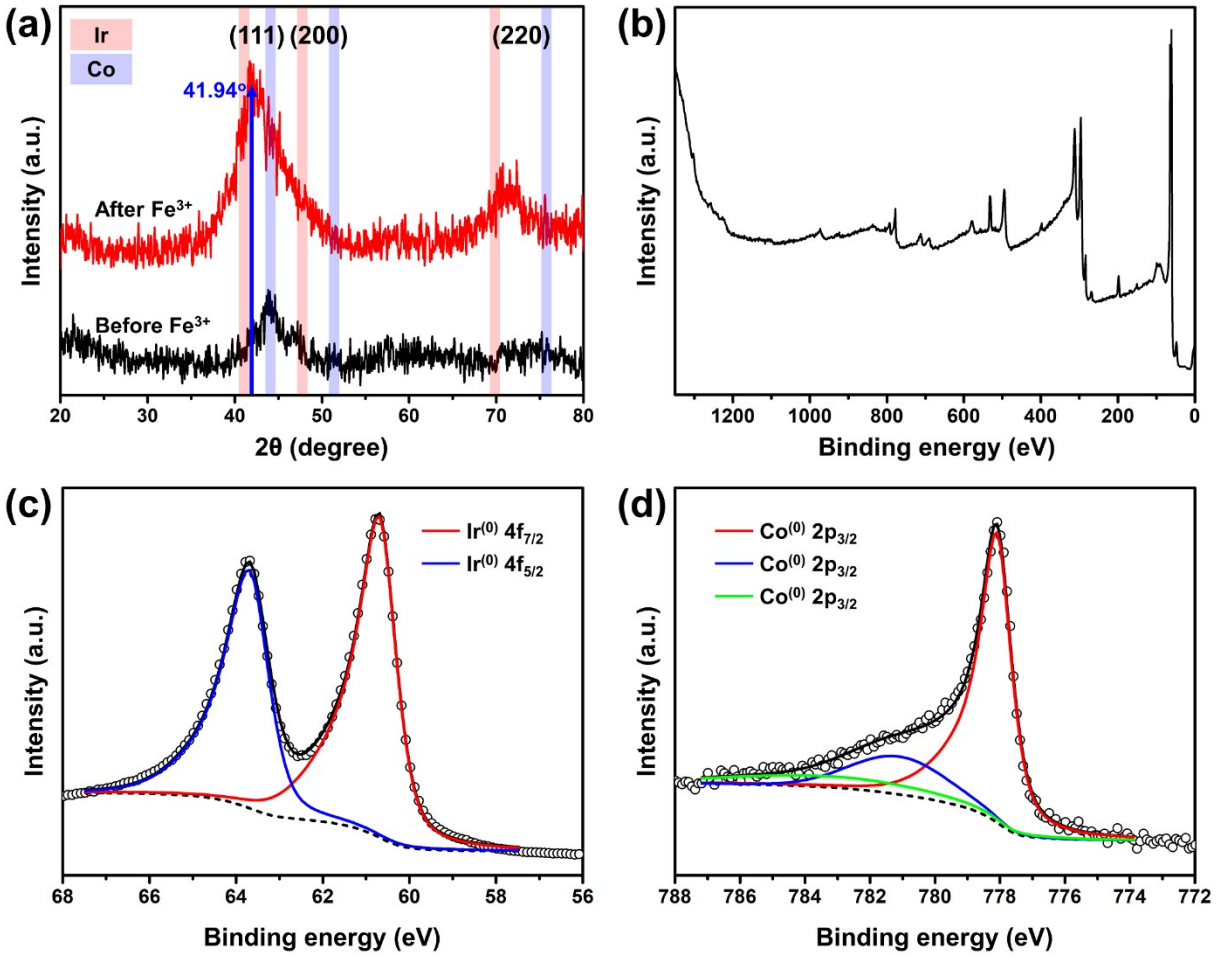

Fig. S10 (a) XRD patterns of Co@Ir core-shell nanoparticles (before Fe^{3+} treatment) (Ir: PDF#01-071-4659; Co: PDF#01-071-4651) and **IC HNPs** (after Fe^{3+} treatment). The blue arrow indicates the 2θ diffraction angle of IrCo(111) in **ICS NCs.** (b) XPS survey spectrum and XPS analysis of **IC HNPs** for (d) Ir 4f and (e) Co 2p.

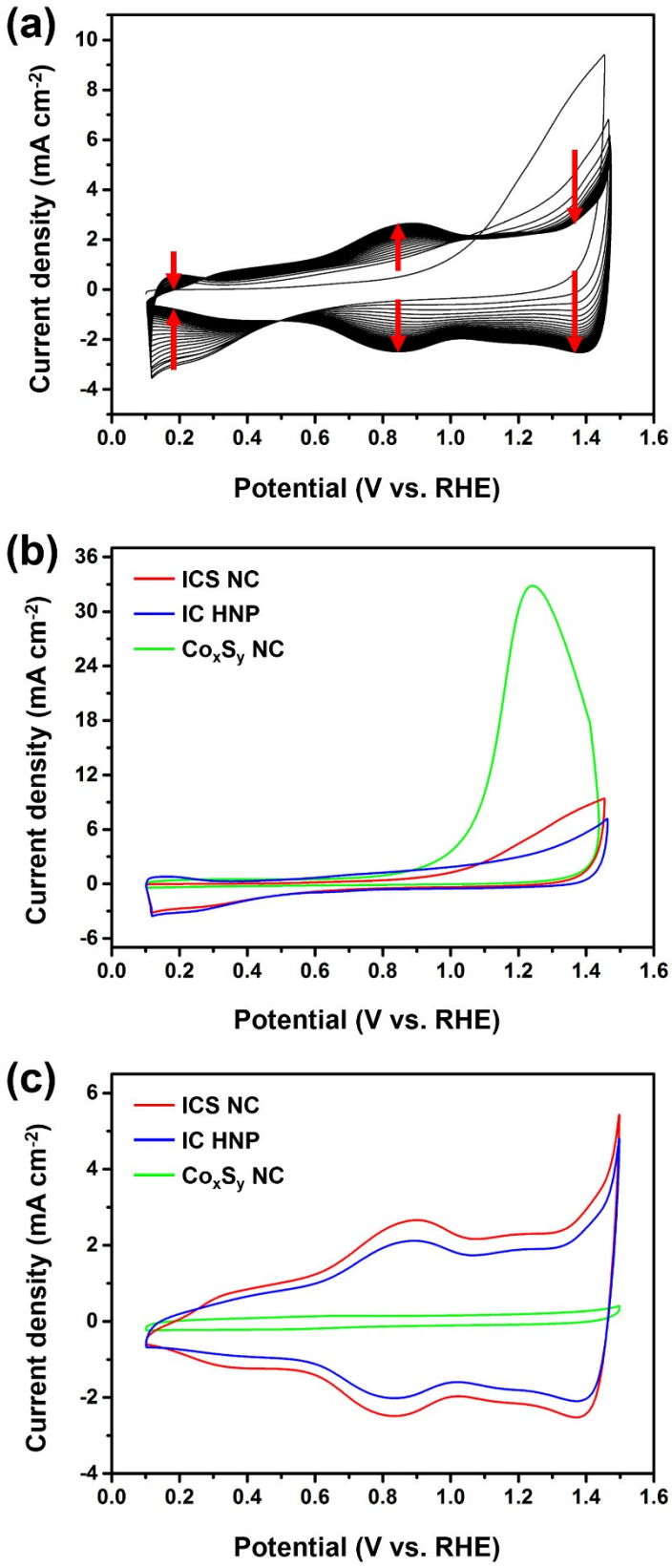

Fig. S11 (a) 40 cycles of CV polarization curves of **ICS NCs** for activation. (b) 1st and (c) 40th cycles of **ICS NCs, IC HNPs** and Co_xS_y nanocages.

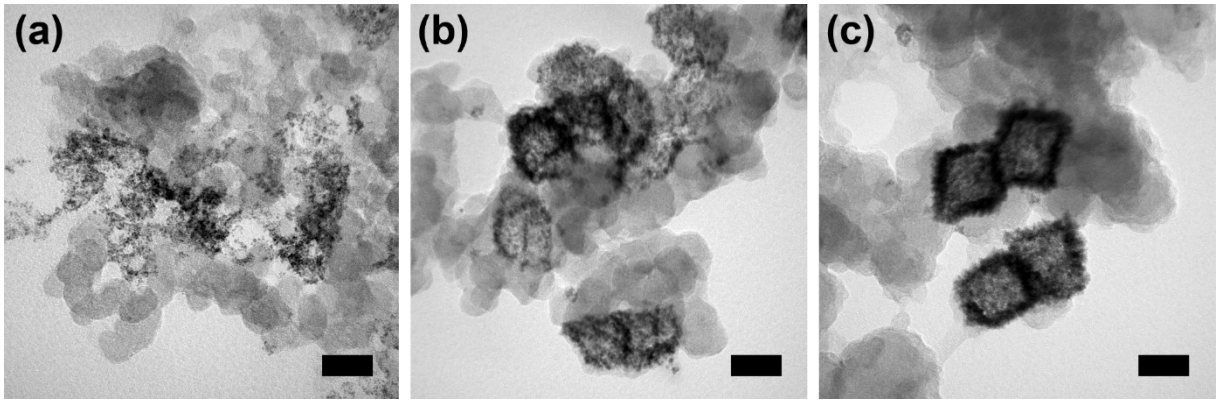

Fig. S12 TEM images of **ICS NCs** synthesized with (a) 0.01 mmol, (b) 0.03 mmol, and (c) 0.06 mmol of Ir precursors after 40 cycles of CV polarization curves. The scale bars are 50 nm.

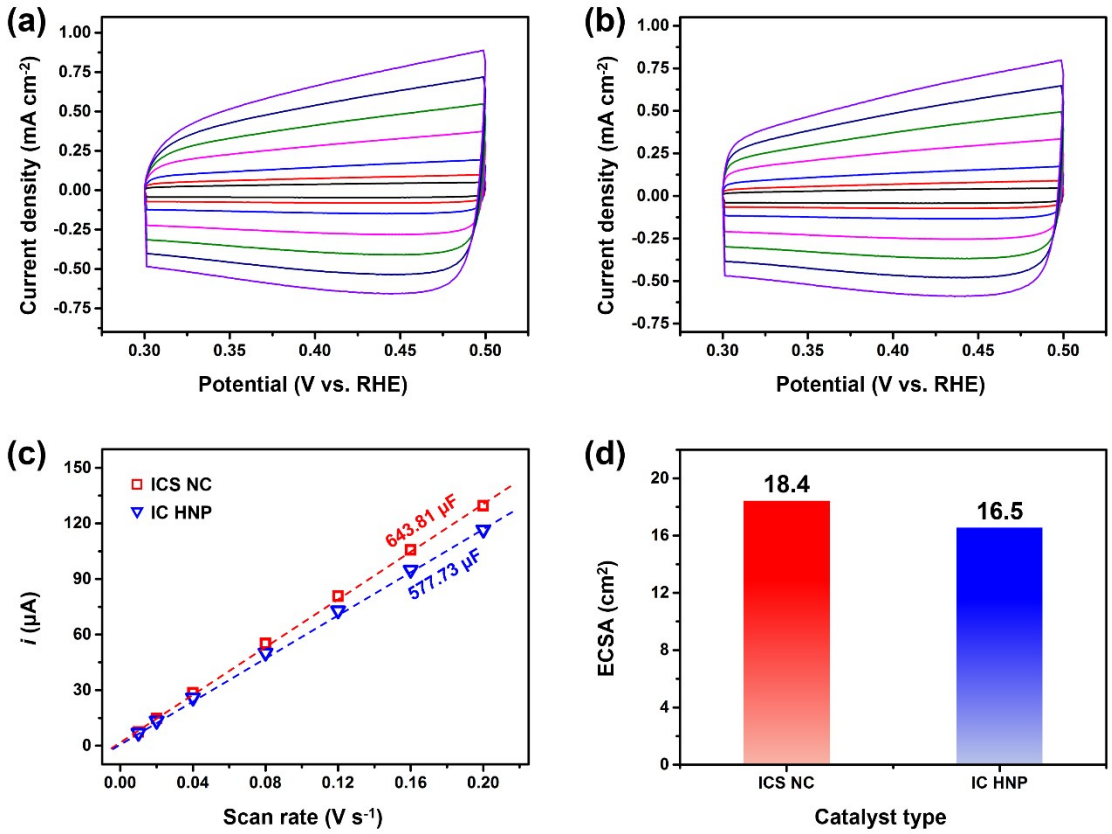

Fig. S13 Electrochemically active surface area (ECSA) by measuring double layer capacitances. CV scans at different scan rates (0.01, 0.02, 0.04, 0.08, 0.12, 0.16, 0.2 V s^{-1}) for (a) **ICS NCs** and (b) **IC HNPs.** (c) Anodic charging currents measured at 0.4 V vs. RHE as a function of scan rate to measure double layer capacitances and (d) the corresponding ECSA values.

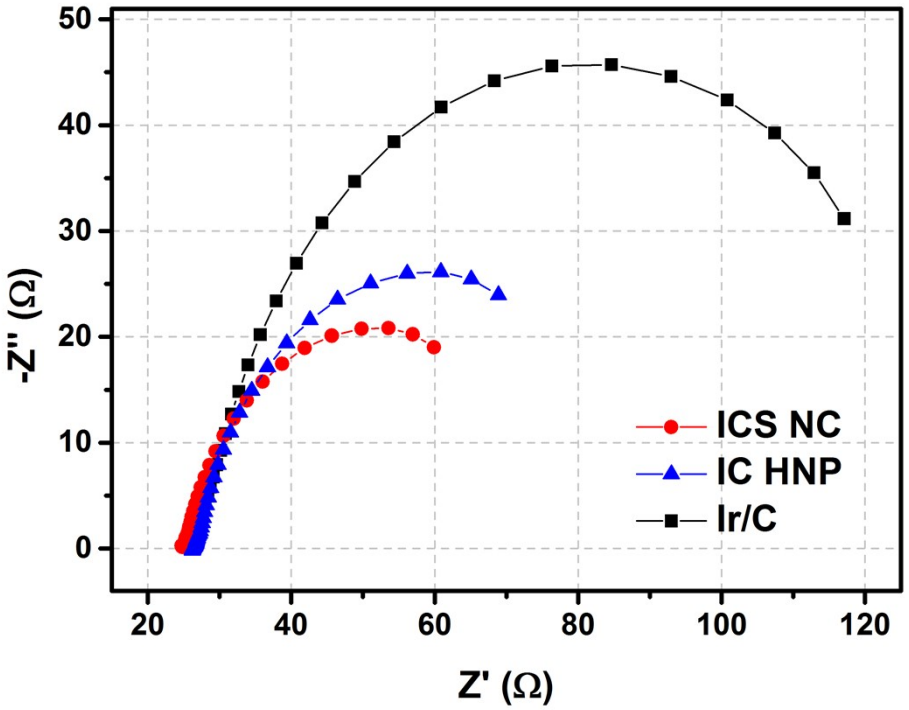

Fig. S14 Electrochemical impedance spectroscopy of **ICS NCs, IC HNPs** and Ir/C.

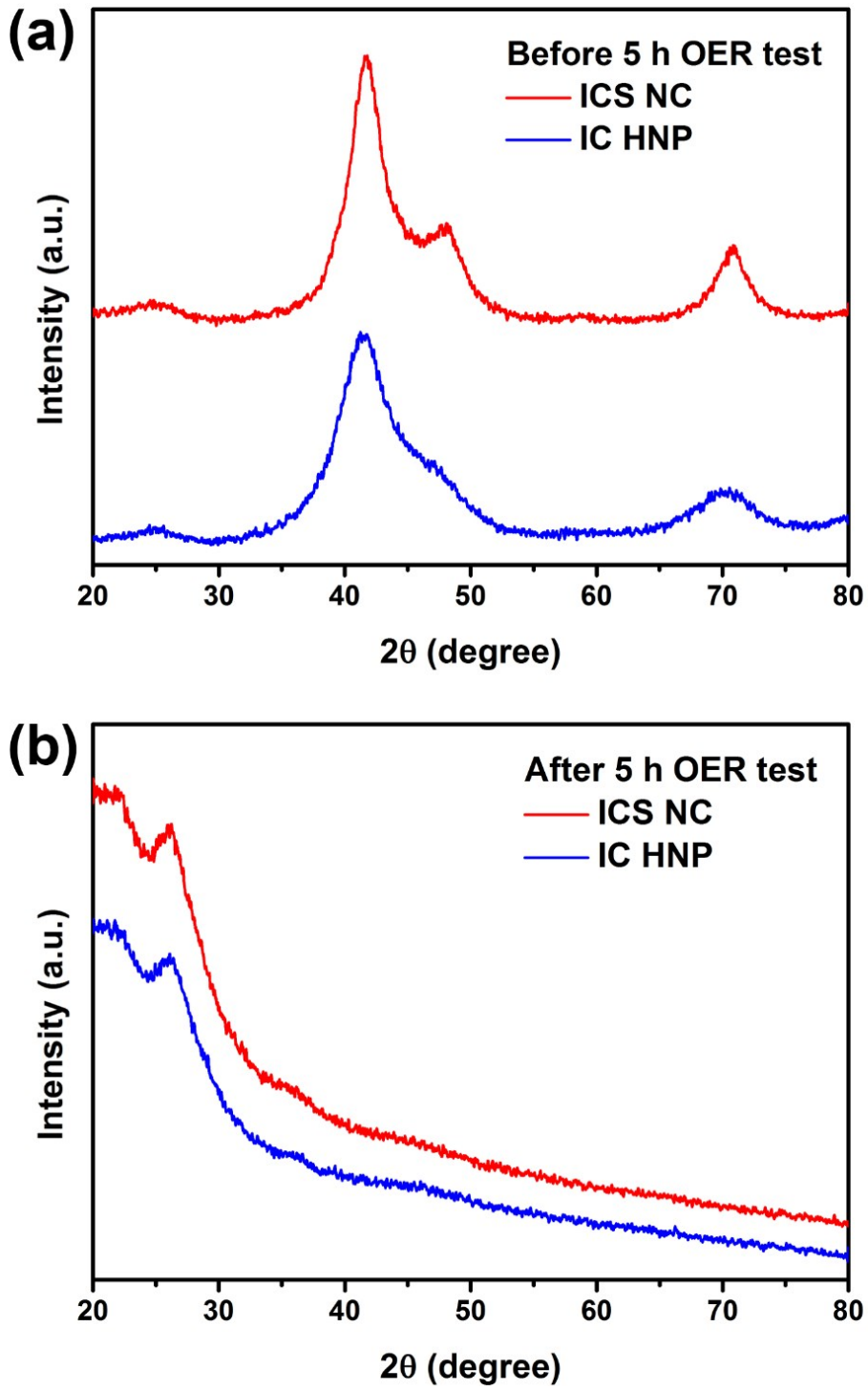

Fig. S15 XRD patterns of **ICS NCs** and **IC HNPs** before and after chronopotentiometry at 10 mA cm^{-2} for 5 h. The peak observed at approximately 25° in both (a) and (b) is assigned to carbon black and the broad peak at 20° in (b) is assigned to polyimide tape which was used to retrieve the catalysts from the glassy carbon disk of RDE.

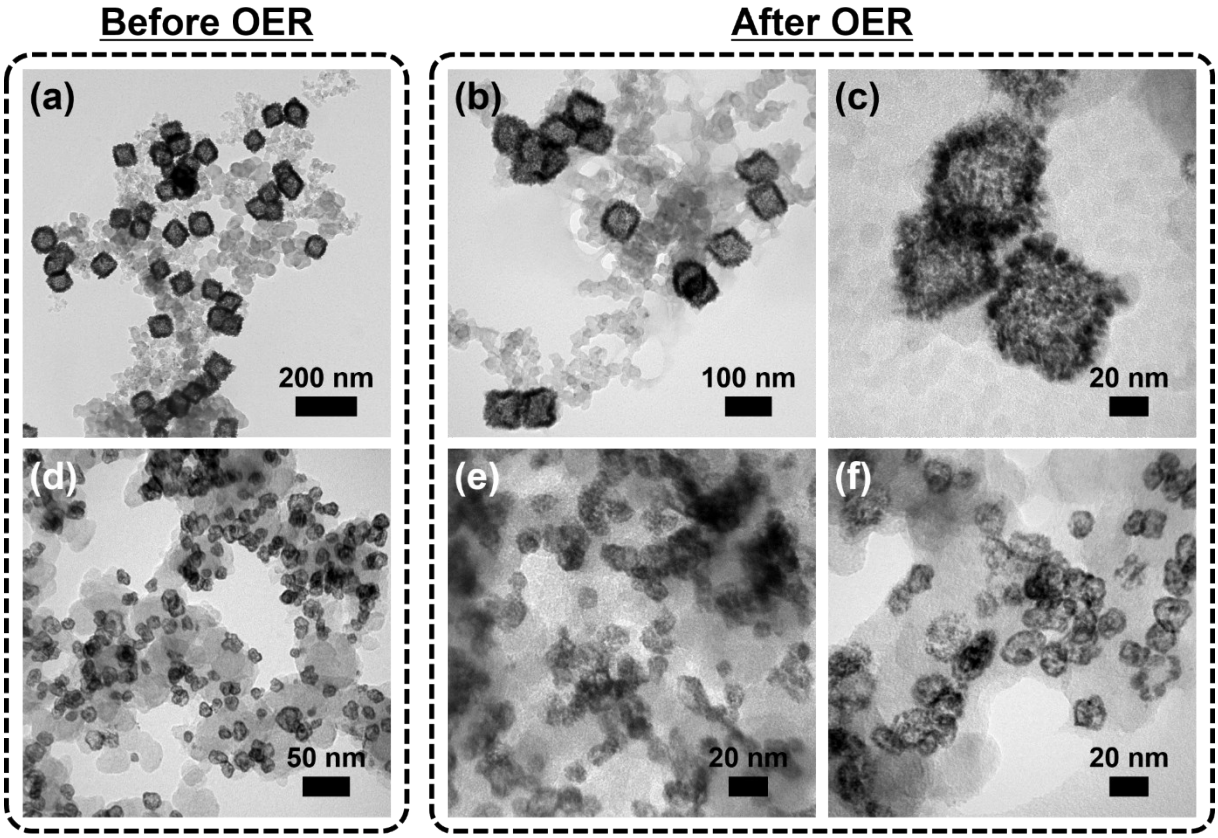

Fig. S16 TEM images of (a-c) **ICS NCs** and (d-e) **IC HNPs** before and after 5 h-chronopotentiometry at 10 mA cm^{-2}.

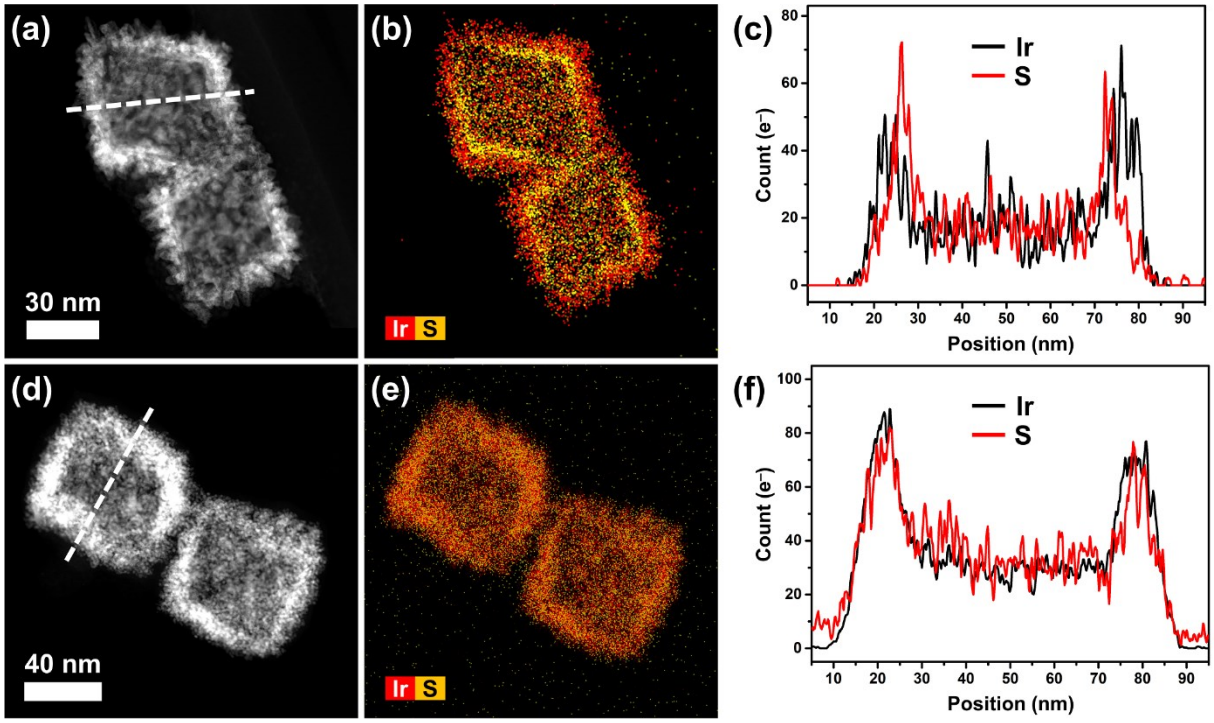

Fig. S17 HAADF-STEM images, elemental mapping images, and line scan profile of **ICS NCs** (a-c) before and (d-e) after 5 h-chronopotentiometry at 10 mA cm^{-2}.

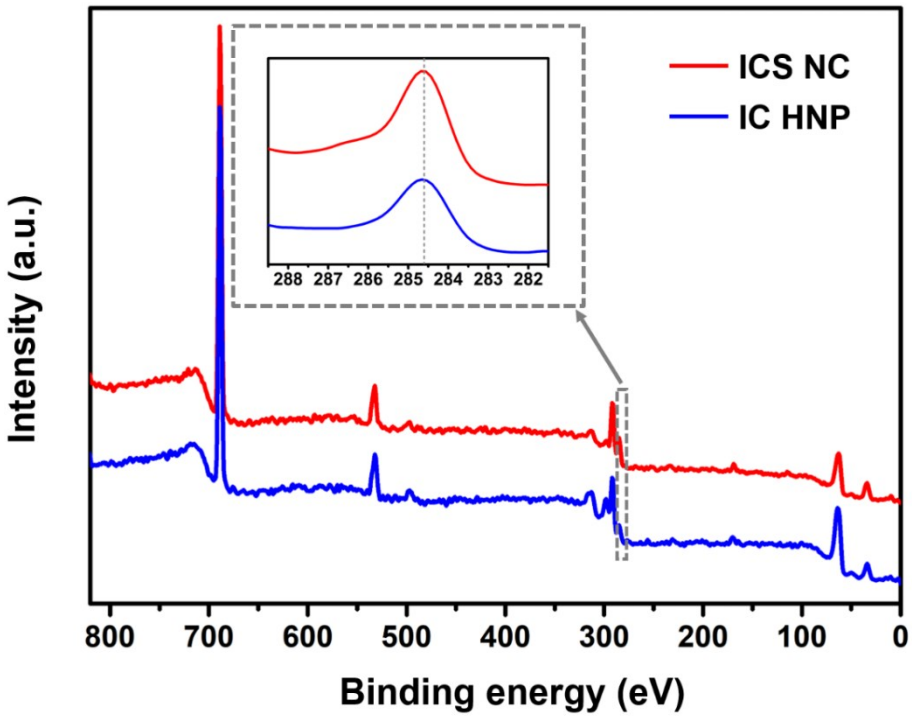

Fig. S18 Survey XPS spectra with an inset of C 1s spectra at 284.6 eV.

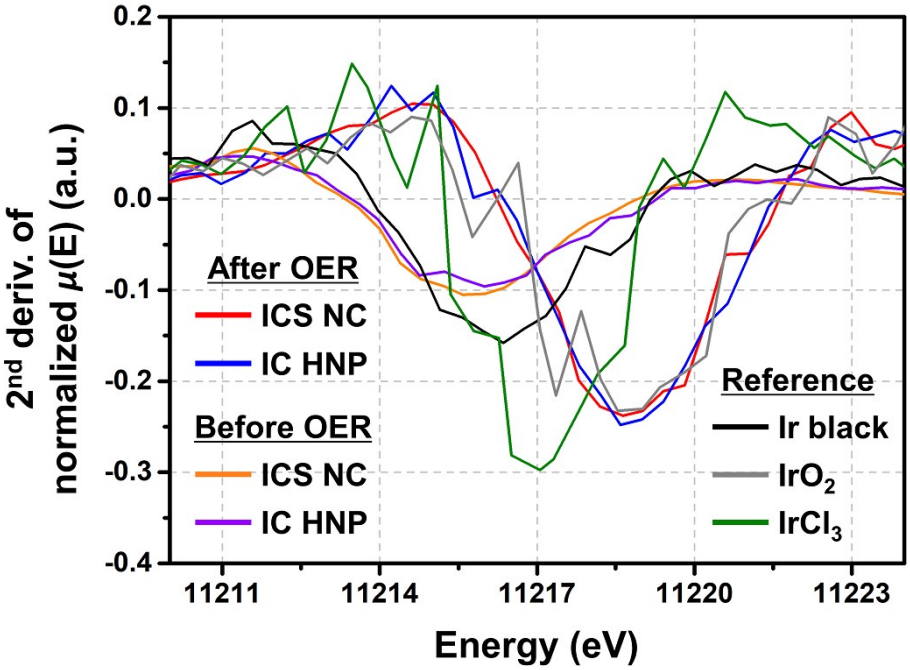

Fig. S19 Second derivatives of Ir L_3-edge XANES regions of **ICS NCs, IC HNPs,** $IrCl_3$, IrO_2 and Ir black.

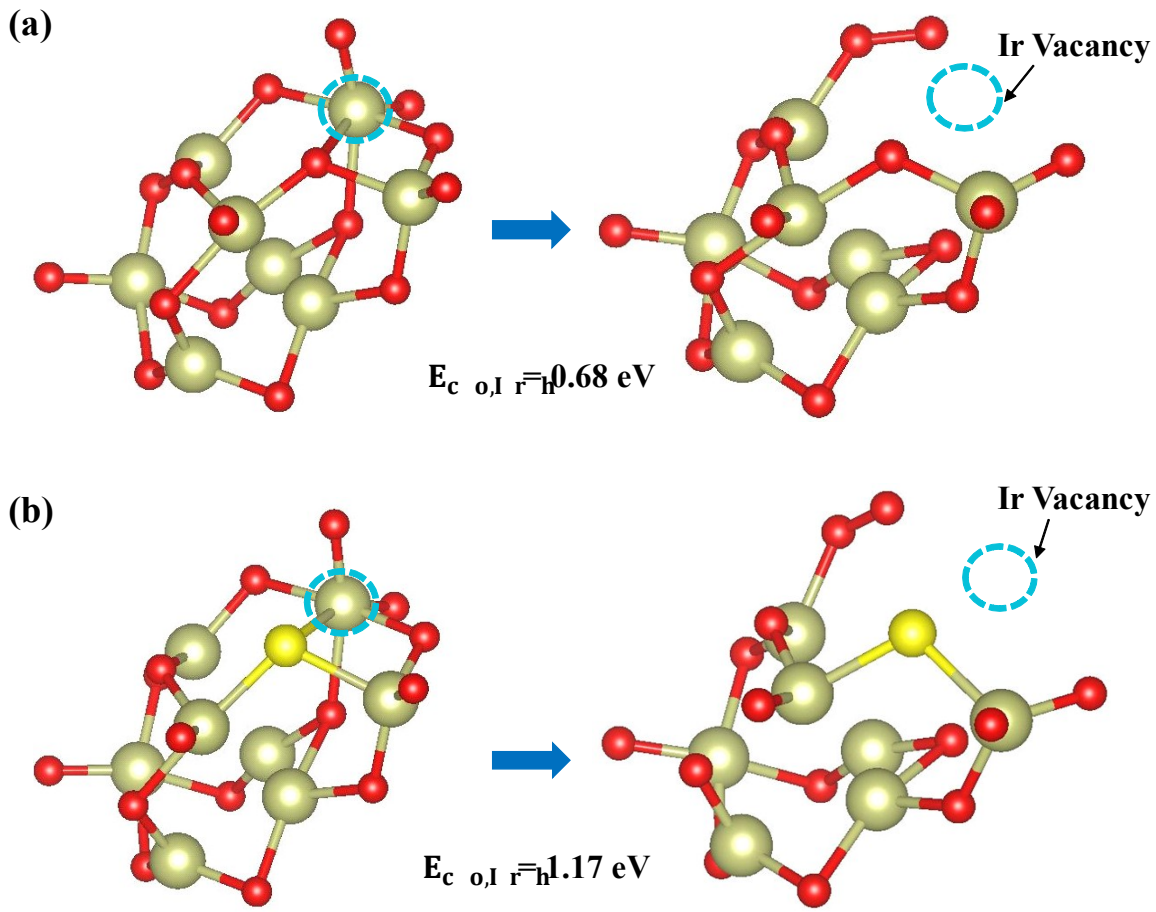

Fig. S20 Optimized geometries of 24-atom (a) pure IrO_2 and (b) S-doped IrO_2 clusters with Ir-vacancy for Δб=2 system. The calculation results for cohesive energy for Δб=2 system are indicated. The grey, red, and yellow spheres represent Ir, O, and S atoms, respectively.

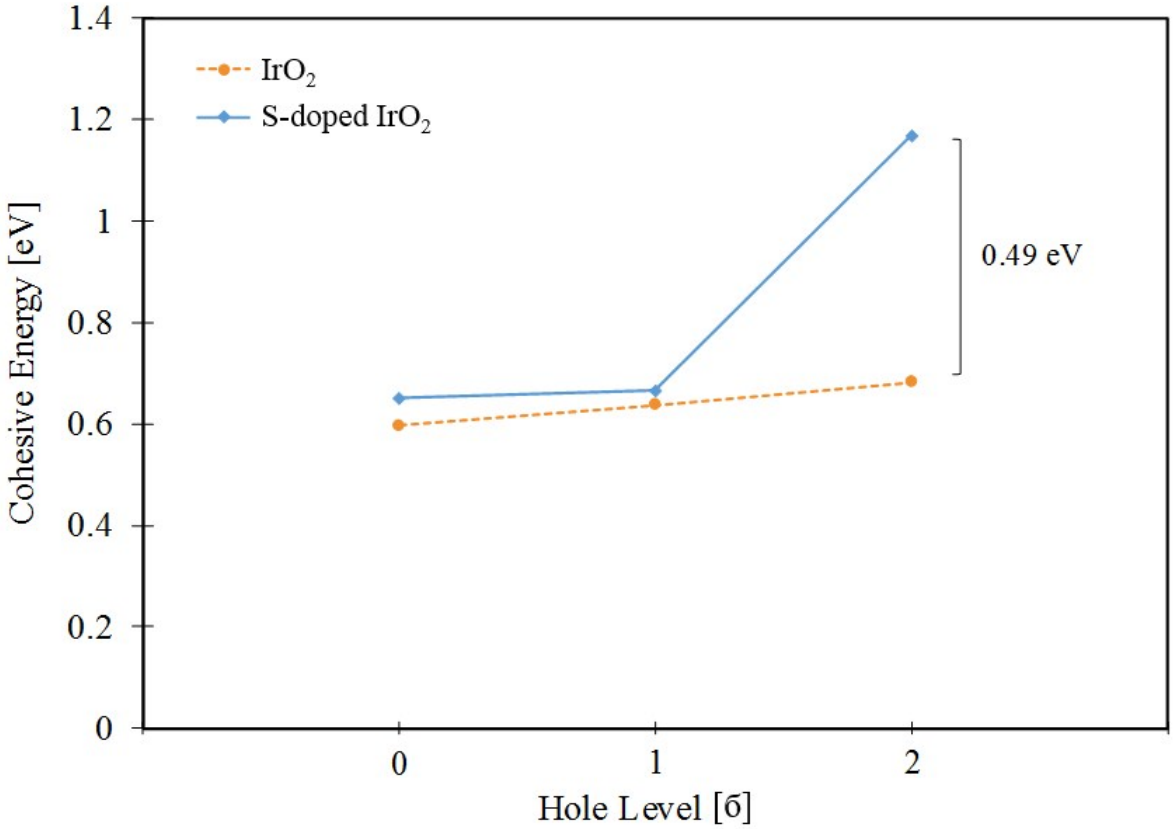

Fig. S21 Calculation results of cohesive energy as a function of hole concentration for IrO_2 and S-doped IrO_2.

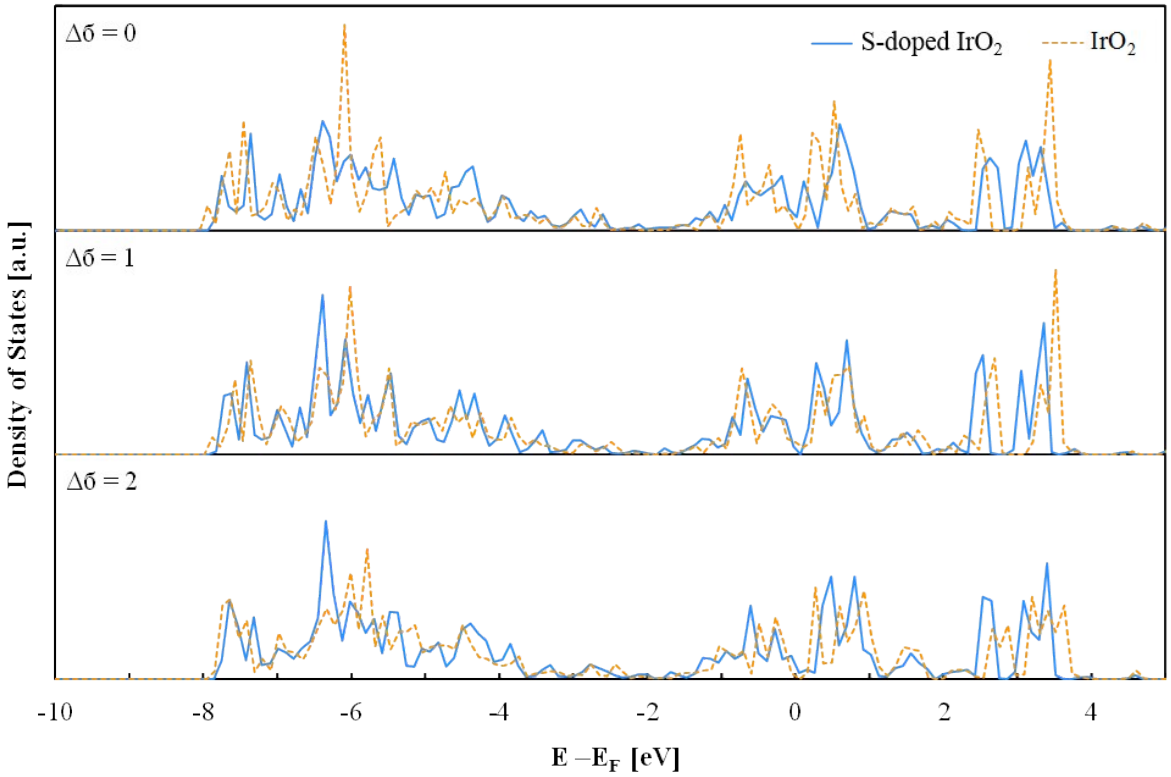

Fig. S22 Density of states (DOS) of Ir atom for IrO_2 and S-doped IrO_2 at different hole concentrations.

Table S1 Comparison of Ir-based electrocatalysts for OER

Catalyst (Nanostructure)	Mass loading (μg_{Ir} cm^{-2})	Electrolyte	Overpotential (mV at 10 mA cm^{-2})	Stability* (CP[a] or ADT[b])	Ref
ICS NC (hollow nanocactus)	15	0.1 M $HClO_4$	281	>100 h at 10 mA cm^{-2}	This work
IC HNP (hollow nanoparticle)	15	0.1 M $HClO_4$	286	~30 h at 10 mA cm^{-2}	This work
Ir (-)	-	1 M H_2SO_4	340	-	2
IrCoNi PHNC (porous hollow nanoparticle)	10	0.1 M $HClO_4$	303	~3.3 h at 5 mA cm^{-2}	5
Co-IrCu ONC (octahedral nanocage)	20	0.1 M $HClO_4$	290	2000 cycles	6
IrNiCu DNF (double nanoframe)	20	0.1 M $HClO_4$	300	2500 cycles	7
IrNi RF (rhombic dodecahedral nanoframe)	-	0.1 M $HClO_4$	313.6	2000 cycles	8
AuCuIrNi-HF (hemi-core/shell nanoframe)	10	0.1 M $HClO_4$	308	24 h at 10 mA cm^{-2}	9
$IrNiO_x$/ATO (core-shell on meso-ATO)	10.2	0.05 M H_2SO_4	360	20 h at 1 mA cm^{-2}	10
IrNi NC (nanocluster)	12.5	0.1 M $HClO_4$	280	~2 h at 5 mA cm^{-2}	11
IrNiFe NP (nanoparticle)	92	0.5 M $HClO_4$	284	~5.5 h at 10 mA cm^{-2}	12
IrO_x/$SrIrO_3$ (thin film)	-	0.5 M H_2SO_4	275	~30 h at 10 mA cm^{-2}	13
Ni-Co doped IrO_2, INC-50 (nanoparticles)	-	0.1 M $HClO_4$	285	~5.5 h at 10 mA cm^{-2}	14
$Ni_{2.53}Ir$ NC (nanocage)	10	0.05 M H_2SO_4	302	10 h at 1 mA cm^{-2}	15

*loading mass of Ir, preparation method and type of working electrode may vary; [a]chronopotentiometry; [b]accelerated durability test; (-) not available

Table S2 Structural parameters of Ir samples and reference samples extracted from the Ir L_3-edge EXAFS fitting. S_0^2 was fixed as 0.61 (Ir black) and 0.87 (IrO_2) during EXAFS fitting, based on the known structure. FT range: k = 3.0 – 13.0 $Å^{-1}$, fitting range: R = 1.1 – 3.0 Å.

Samples	Scattering pathway	Coordination number	ΔE_0 (eV)	R (Å)	σ^2 (10^{-3}×$Å^2$)	R-factor
Ir black	Ir-Ir	12	5.69 ± 1.85	2.70 ± 0.01	4.6 ± 1.1	0.017
IrO_2	Ir-O	6	9.31 ± 1.30	1.99 ± 0.01	5.8 ± 1.3	0.014
IC HNP after 5 h OER	Ir-O	4.8 ± 0.6	9.52 ± 1.95	2.00 ± 0.01	5.0 ± 1.7	0.018
	Ir-Ir	4.6 ± 2.3		2.69 ± 0.02	9.0 ± 3.5	
ICS NC after 5 h OER	Ir-O	3.1 ± 1.1	-0.94 ± 1.85	2.02 ± 0.03	7.7 ± 5.3	0.005
	Ir-S	0.6 ± 0.2		2.16 ± 0.02	9.6 ± 2.6	
	Ir-Ir	6.6 ± 1.3		2.64 ± 0.01	8.8 ± 1.1	

SUPPLEMENTARY REFERENCES

1. J. Kim, H. Jin, A. Oh, H. Baik, S. H. Joo and K. Lee, *Nanoscale,* 2017, **9,** 15397-15406.
2. C. C. L. McCrory, S. Jung, I. M. Ferrer, S. M. Chatman, J. C. Peters and T. F. Jaramillo, *J. Am. Chem. Soc.,* 2015, **137,** 4347-4357.
3. B. Ravel and M. Newville, *J. Synchrotron Rad.,* 2005, **12,** 537-541.
4. S. I. Zabinsky, J. J. Rehr, A. Ankudinov, R. C. Albers and M. J. Eller, *Phys. Rev. B,* 1995, **52,** 2995-3009.
5. J. Feng, F. Lv, W. Zhang, P. Li, K. Wang, C. Yang, B. Wang, Y. Yang, J. Zhou, F. Lin, G.- C. Wang and S. Guo, *Adv. Mater.,* 2017, **29,** 1703798.
6. T. Kwon, H. Hwang, Y. J. Sa, J. Park, H. Baik, S. H. Joo and K. Lee, *Adv. Funct. Mater.,* 2017, **27,** 1604688.
7. J. Park, Y. J. Sa, H. Baik, T. Kwon, S. H. Joo and K. Lee, *ACS Nano,* 2017, **11,** 5500-5509.
8. H. Jin, Y. Hong, J. Yoon, A. Oh, N. K. Chaudhari, H. Baik, S. H. Joo and K. Lee, *Nano Energy,* 2017, **42,** 17-25.
9. J. Park, S. Choi, A. Oh, H. Jin, J. Joo, H. Baik and K. Lee, *Nanoscale Horiz.,* 2019, **4,** 727-734.
10. H. N. Nong, H.-S Oh, T. Reier, E. Willinger, M.-G. Willinger, V. Petkov, D. Teschner and P. Strasser, *Angew. Chem. Int. Ed.,* 2015, **54,** 2975-2979.
11. Y. Pi, Q. Shao, P. Wang, J. Guo and X. Huang, *Adv. Funct. Mater.,* 2017, **27,** 1700886
12. L. Fu, G. Cheng and W. Luo, *J. Mater. Chem. A.,* 2017, **5,** 24836-24841.
13. L. C. Seitz, C. F. Dickens, K. Nishio, Y. Hikita, J. Montoya, A. Doyle, C. Kirk, A. Vojvodic, H. Y. Hwang, J. K. Norskov and T. F. Jaramillo, *Science,* 2016, **353,** 1011-1014.
14. W. Q. Zaman, Z. Wang, W. Sun, Z. Zhou, M. Tariq, L. Cao, X.-Q. Gong and J. Yang, *ACS Energy Lett.,* 2017, **2,** 2786−2793.
15. C. Wang, Y. Sui, M. Xu, C. Liu, G. Xiao and B. Zou, *ACS Sustainable Chem. Eng.,* 2017, **5,** 9787−9792.